Micro-movements of Implant-abutment-interface

Test-Report

(Champions Implant (R)evolution 4,5)

Department of Prosthetic Dentistry

J. W. Goethe-University Frankfurt am Main

Director: Prof. Dr. H.-Ch. Lauer

Dipl.-Ing. H. Zipprich

Address:

Theodor-Stern-Kai 7,Haus 29

60596 Frankfurt a. Main

Date: **13. August 2012** Fax: (069) 6301-3711

E-Mail: Zipprich@em.uni-frankfurt.de Fon: (069) 6301-4714

Directory

1 Material and method

In order to examine the existence of a microgap on dental implants; a special experimental test field was developed. For each type of implant-system tested; five inspection pieces were manufactured. Each inspection piece simulates an implant-supported molar crown in the upper jaw. During the load, in a two-dimensional chewing simulator, a constant and diverging X-ray device radiated the inspection pieces. By transformation of the x-ray into visible light; x-ray videos were recorded, using a high speed digital camera. The results will give information on the development and a conclusion of a microgap at the implant abutment interface.

2 Experimental setup

Illustration 1 shows schematically the experimental setup. Those in the x-ray source: [1] analysation of an exemplary inspection piece loaded in a two-dimensional chewing simulator [3] [2; 4]. The x-rays are converted in the image amplifier [5] into visible light. The quantity of light coming from the image amplifier meets the CCD sensor of the High speed digital camera [6]. Afterwards; the camera sends a digital signal to an attached computer, whereas the computer then developes x-ray-videos on the processes of the Implant-Abutment-Interface.

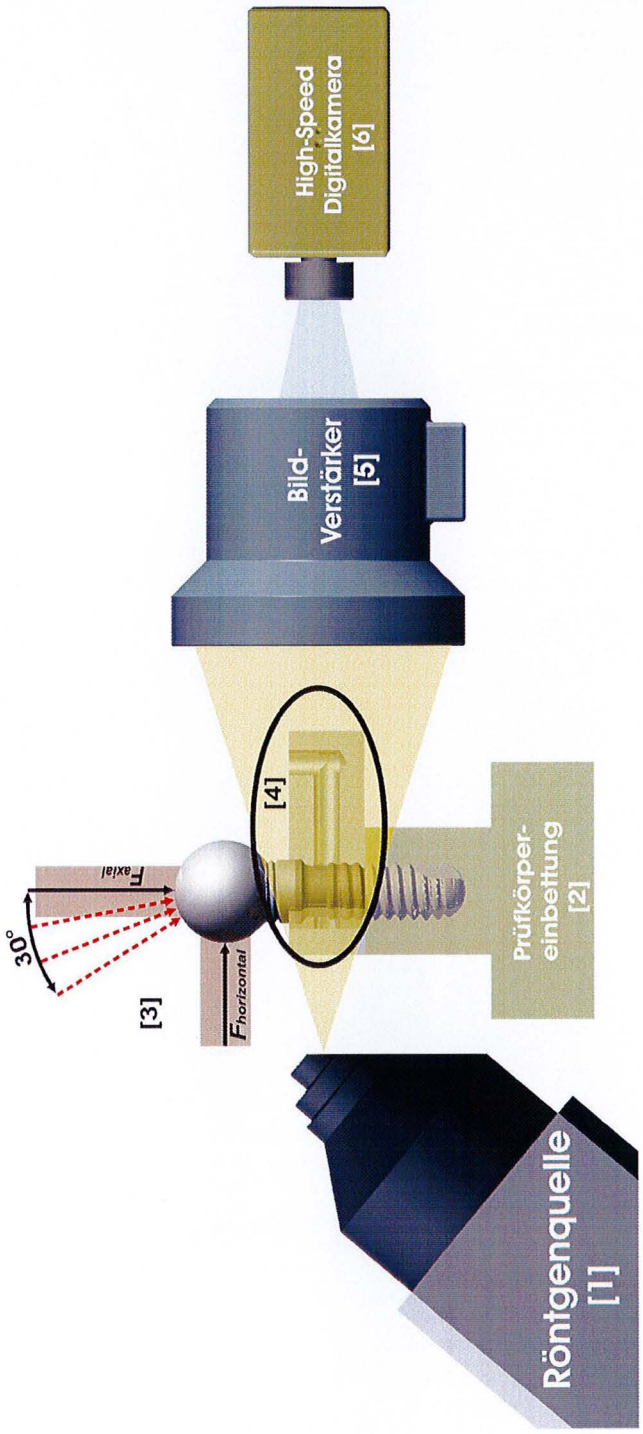

Fig. 1:
Schematic representation of the experimental setup.
[1] = source of x-ray
[2] = embedded inspection piece
[3] = chewing simulator
[4] = saliva replacement/ x-ray contrast medium
[5] = radiograph amplifier
[6] = High speed digital camera

2.1 Source of x-ray

In the, here described, investigation an x-ray unit type FXS-160.50 was used. (Fine focus of X-Ray systems, www.yxlon.de). Fig. 2 shows a schematic diagram of the x-ray unit used.

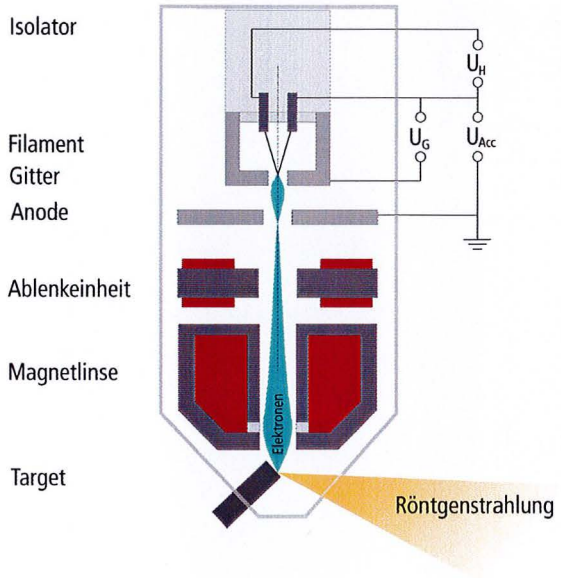

Fig. 2:
Schematic structure of the x-ray tube.

Used specific data for the source of x-ray are the Tab. to infer 1a and b.

Radiation characteristic	▪ Emission angle: 40° ▪ rotational target Target material: Tungsten with beryllium filter

Tab. 1a: Specific data of the x-ray source.

Ranges	▪ Tension 5 - 160 kV ▪ Target stream 0 - 1,0 mA ▪ Continuous duty (+ Cooling): 160 Watt ▪ Focal spot size adjustable 3 - 1000 µm

Tab. 1b: Specific data of the x-ray source.

The applied x-ray unit is a constant emitter, with which the x-radiation spreads divertingly. Divertional spreading of the radiation, leads to an enlargement of the radiated object (see fig. 3).

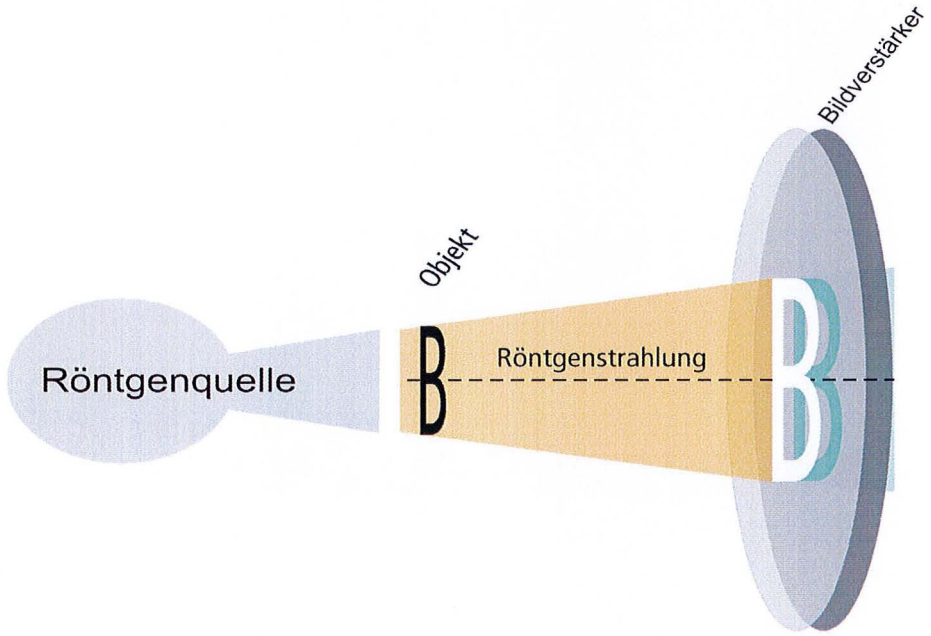

Fig. 3: Geometrical conditions the object radiograph amplifiers of source of x-ray.

The focal spot size can be adjusted up to 3 µm (Tab. 1) and therefore leads to a theoretical resolution of maximum 3 µm. To note though is however; that the bulb *power* needs to reach 16 Watts, to allow for a manually adjustment of the focal spot of 3 µm. The increase and achievement of over 16 Watts automatically leads to an enlargement of the focal spot and concomitantly reduction of the resolution. In the investigation; a maximum output of 16 Watts was used. A lead screen was used to avoid stray radiation.

In the available test series; an underlying closed voltage of 120 keV and a current of 0,1 mA was used. The output is calculated with and results in 12 Watts.

2.2 *Inspection piece*

Tab. 2 shows the tested implant-components.

Compnents	**measurement**	**reference no.:**
Champions Implant (R)evolution	D 4.5 L 12.0	0850
Abutment 0^0 (R)evolution GH3		31050

Tab. 2: tested implant-components.

2.3 *Production of the inspection pieces*

The production of the inspection pieces required some preparing measures, which are explained in the following:

Production of cementation caps

The cemented caps consist of aluminium, which were applied on each abutment by means of attachment; using autopolymerizing composits (3M Espe Nimetic™ Cem; www.espe.de). The manufacturing of all cemented caps took place through a centrifical lathe (company emco Austria, emcotronic TM02 and emco turn 120). The aluminium caps have an inside diameter of 3,5mm, are 6mm in length and have an internal thread (M5 x 0,5mm) of variable length. Fig. 4 shows exemplarily two cementing caps. The caps serve as assistance for the screwing of the load attachments, which are described in the following.

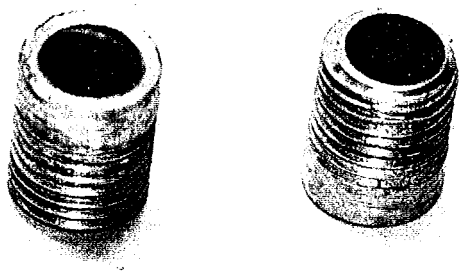

Fig. 4: Cementing caps from aluminum.

Preparation of the Abutments

The original abutments were manufactured under manufacturing specifications and diameters (see Tab. 2). For the available investigation all abutments were milled to a diameter of 3,45mm in a centre lathe (company emco Austria, emcotronic TM02 and emco turn 120). Subsequently, all abutments were sandblasted carefully with commercial blasting equipment. This measure served as reinforcement for the glued connection between the cementing cap and the Abutment. Fig. 5a shows an exemplary abutment before milling, whereas fig. 5b shows the same Abutment after lathing and sand blasting.

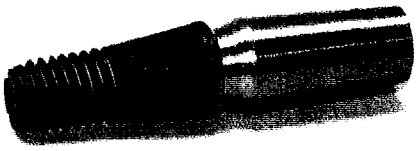

Fig. 5a: Implant with a non-milled original Abutment.

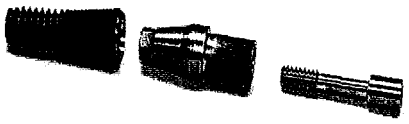

Fig. 5b: Implant with a milled and blasted Abutment including the fixation screw.

Assembly of the Abutments

The milled and blasted Abutments were fixed to the implant using the manufacturer's specificaitions (Champions Implant 30 Ncm). A calibrated torque wrench Torsiometer 760 (www.stahlwille.de) was thereby used. Fig. 6 shows the torque wrench used and all recommended manufacturing tightening torques were followed.

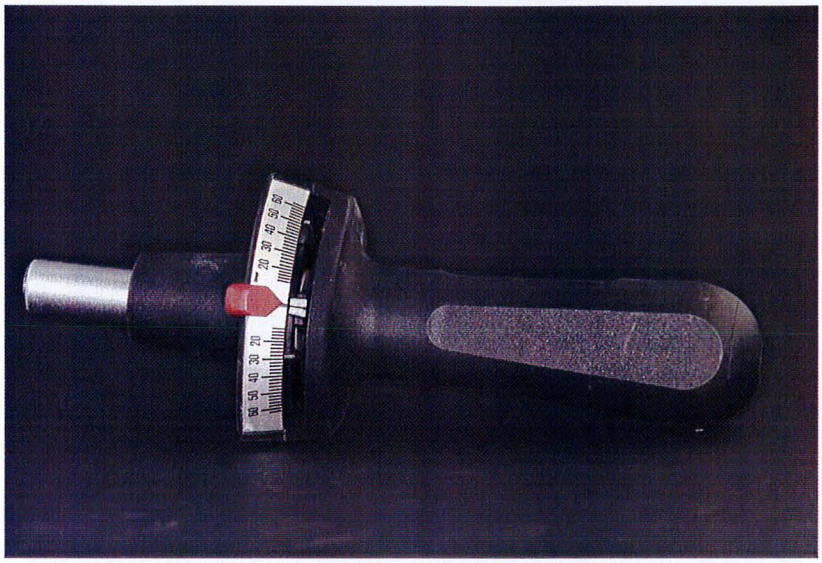

Fig. 6: calibrated torque wrench.

Production of the load attachment

The load attachment for the enossale implant abutment was designed spherically. A loading ball cap attachment was manufactured for each inspection piece. The ball attachment consists of aluminum and has an outside diameter of 8,0mm. In fig. 7 a load attachment (loading ball cap) is represented.

Fig. 7: load attachment.

The internal thread of the load ball fits the external thread of the cementing cap. This allows for a variable length of the ball height and an adjustment of the lever arm length. Fig. 8 shows the load attachment screwed onto the cementing cap. In order to ensure a firm seat of the spherical load attachment, a PTFE sealant strip was applied on the external thread of the cementing cap.

Fig. 8: Cementing cap with a screwed on load attachment.

Production of the embedding mold

In order to standardise the embedding of the implants; an embedding mold was manufactured for all units tested. The production of the mold always followed same protocol. A T-fitting block of aluminum (T1) was manufactured for each implant system. The block (T2) served as negative for the manufacturing of the T-fitting units using Technovit® 4004, in which each implant tested was embedded. In T1 a preparatory implant was set. The positioning and measurements used are shown in Fig. 9.

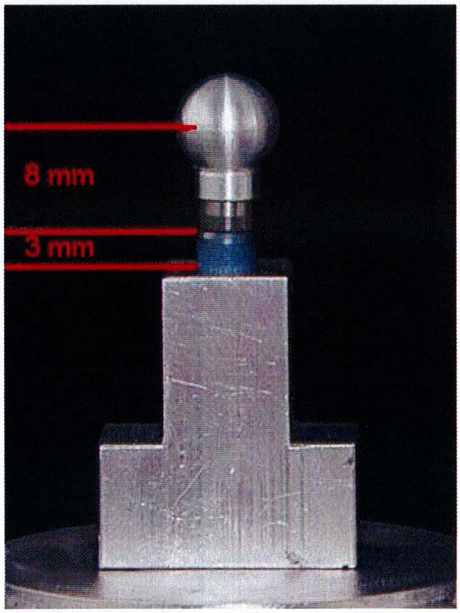

Fig. 9: In the T-fitting (T1) positioned implant.

The embedding form was manufactured using silicon (Copie sil® 18 basis and catalyst, dentona AG Dortmund). In addition; a cylindrical-form using aluminum was designed and manufactured as a container for molding. The designated implant was attached at the base of the cylindric-form T1, (Fig. 10), using a screw fixation.

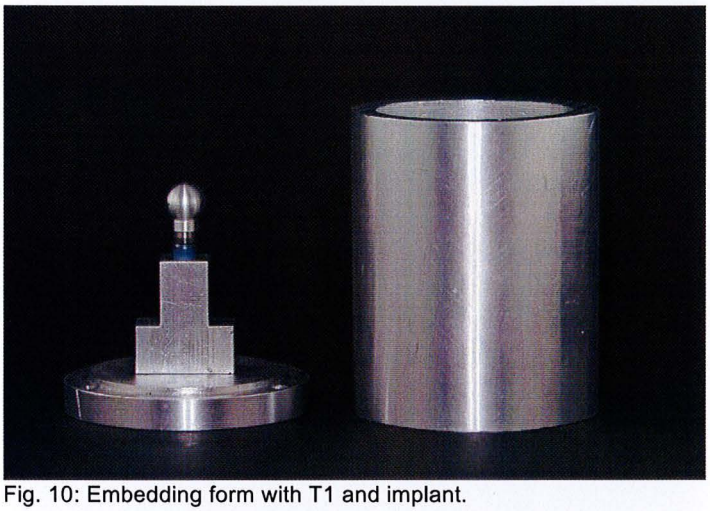

Fig. 10: Embedding form with T1 and implant.

After attachment and screw fixation, the cylindrical-form was then filled from above using silicon (Copie sil® 18 basis and catalyst, dentona AG Dortmund) in (fig. 11).

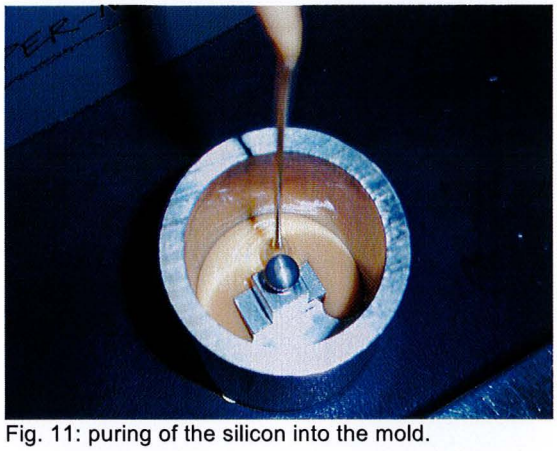

Fig. 11: puring of the silicon into the mold.

After disassembly of the cylindrical-form and removal of the base, by loosening of the retention screws from T1, the T-fitting unit could be easily removed from the manufactured embedding mold, due to the high elasticity of the silicon. Such a mold served as embedding device for each individual implant, so that an embedding mold was

manufactured for the implant system. In Fig.12a and b the sectional view of an embedding mold is shown.

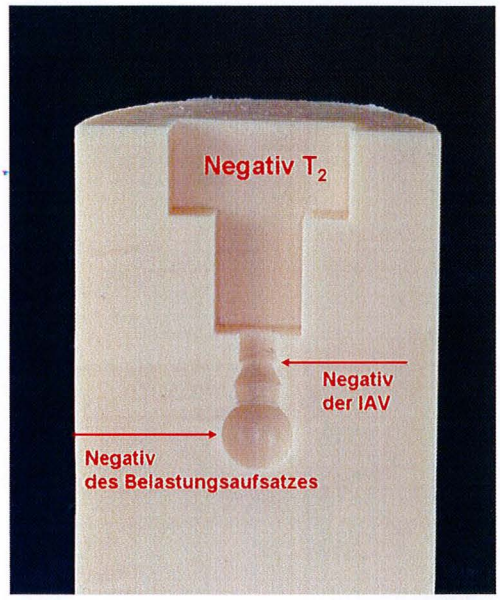

Fig. 12 a: Sectional view of an embedding mold.

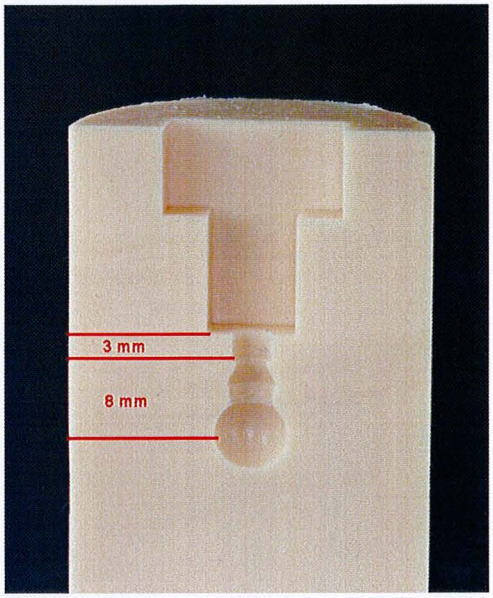

Fig. 12 b: Distances within the embedding mold. Representation for the norm DIN 14801.

Each implant in the study was prepared using the descriptive approach for the embedding of the implant bodies.

The implant body embedding

The result of the preparation measures is a system-specific embedding process, for an enossal implant with a definitely attached abutment. On this prosthetic post the cementing cap is fastened and the load attachment is screw-fixed in such a way that the measurements requirements are fulfilled; as shown in fig. 12 b. In fig. 13 finally prepared implant is to be shown.

Fig. 13: Champions Implant (R)evolution Implant with cemented cap and load attachment (ball).

With the help of the manufactured molds the implants could be embedded, using the transparent, 2-component material on basis of Methylmethacrylat, in form of powder and liquid (Technovit® 4004; www. kulzer technik.de). The screwed ball cap (load attachment) ensures an accurate positioning of the implant in the embedding mold (fig.14a and b).

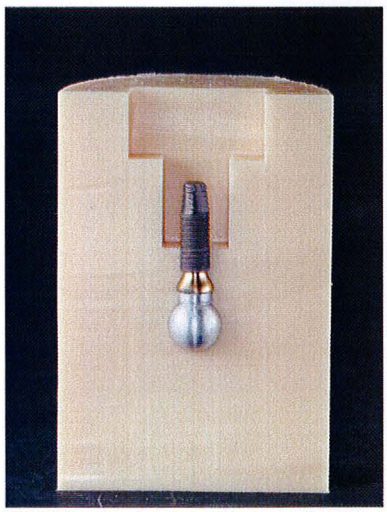

Fig. 14a: Implant positions in the embedding mold; Sectional view. Fig.

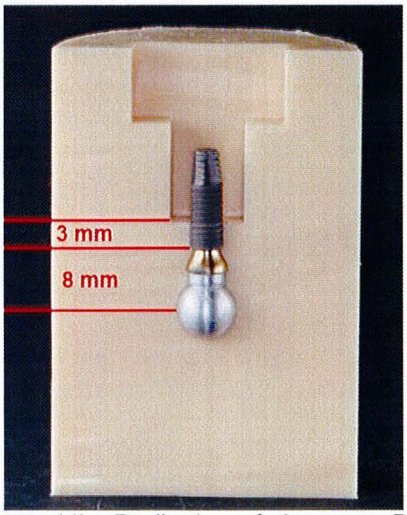

Fig. 14b: Realization of the norm DIN 14801.

After positioning of the implant in the embedding mold, the cavity (T-fitting) was filled with resin (Technovit® 4004; www.kulzer-technik.de). Fig. 15 shows an implant in the embedding mold and Fig. 16 shows the filling of the cavity with resin.

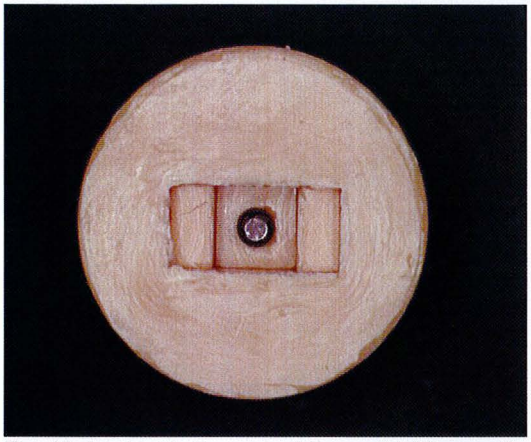

Fig. 15: Implant in the embedding mold; View on the apical portion of the implant.

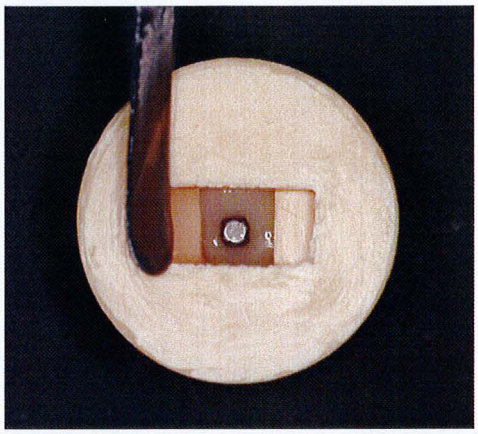

Fig. 16: Filling of the embedding mold with resin.

After the polymerization (manufacturer data 4-6 min.) the implant was firmly embedded in the resin and could be removed from the form. Fig. 17 represents an implant after removal from the mold. The load distance, defined by the distance from the ball center up to the implant shoulder, is a consistant 8mm (tolerance +/− 0,1mm). The height of the embedded implant body corresponds to the portion of the implant, which is clinically embodied in the bone. Following the DIN EN ISO 14801 a boneloss was of 3mm was simulated.

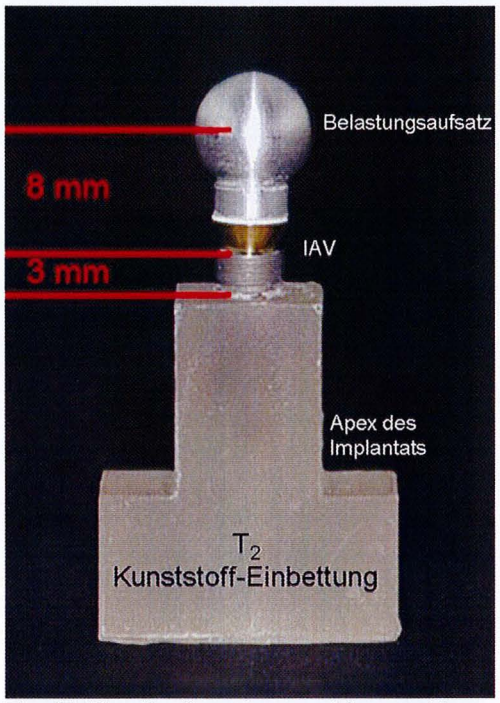

Fig. 17: Directly after releasment from mold. Embedded implant with load attachment (ball cap). DIN 14801 illustration.

This embedding-material was selected because its' module of elasticity (elastic module) of approximately 2000 - 2300 N/mm2 (Technovit® 4004, www.kulzer-technik.de) and is therefore a little over the value of Human Spongiosa. Human bone values are known to be between 1000 N/mm2 (Spongiosa) and 10000 N/mm2 (Cortical). In the herein examined study an implant-supported molecular crown of the upper jaw was simulated. The maxilla consists in large of Spongiosa; whereas the Corticalis, with its' compact structure, constitutes only a small portion. Therefore the Corticalis under clinical conditions surrounds a smaller part of the implant body than the Spongiosa. Elastic module of the herein used embedding-material was selected so that it resembles the elastic module of the Spongiosa. The influence factor of the Corticalis was thereby considered.

2.4 Chewing simulator

In the available investigation a two-dimensional chewing simulator was used. „The Frankfurt chewing simulator "was designed and built particularly for testing of Implant Abutment connections (IAI). It makes the application of two-dimensional chewing forces possible. On the inspection samples and/or on the IAI, the influencing force is produced by two electro-dynamic force actuators. These are arranged in right-angles to one another in the „Frankfurt chewing simulator " (Fig. 18).

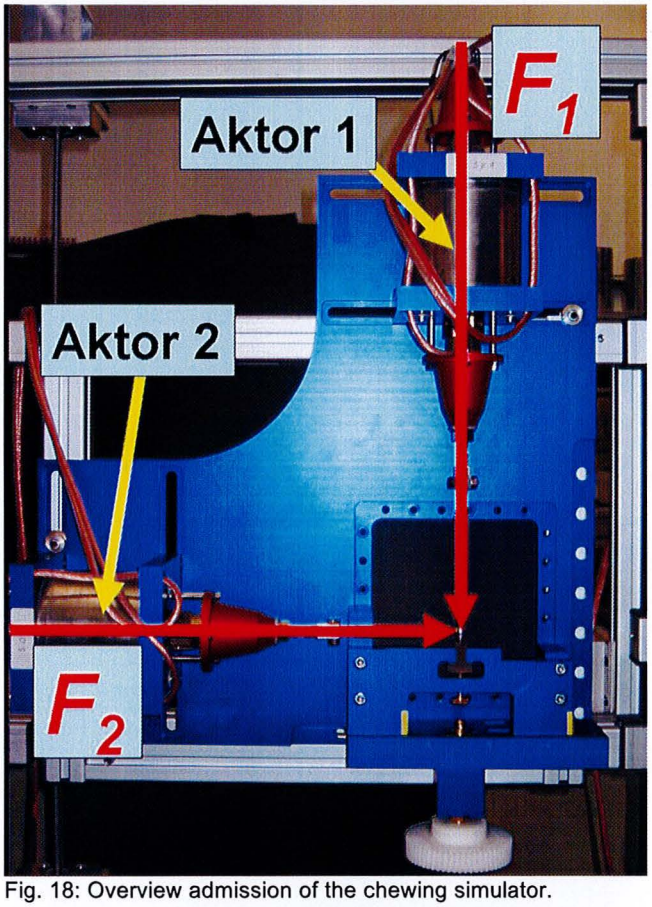

Fig. 18: Overview admission of the chewing simulator.

The force-time-process is variable and adjustable in the used actuators. Both actuators use the Lorenz strength, for which the following formula is the basis.

$$F_{(t)} = i_{(t)} \times l \times B$$

F (t) = time-dependent Kraft (Lorenz Kraft) [N]
i (t) = temporally changeable river [A]
l = effective leader length [mm] B = magnetic flow density [C]

From the mathematical context; there is a relationship between the actuator stream (coil stream) and the produced force. The actuator stream is therefore directly proportional to the produced force. The simultaneous, however independent force production in both force actuators makes for total produced force of between 0-300 Newton possible. The generated force can be introduced in arbitrary directions of +90° to −90° related to the implant axis. The tolerance of the force actuators amounts to 0.5%. This was determined with force sensors. The two force actuators are controlled through an electronic amplifier (www.willburger.de). The control of the amplifier is driven through a digitally/similar transducer map (company national instrument, type NI USB 6229), which is controlled and directed by the use of the graphic programming system LabVIEW® (www.ni.com). Acceleration changes of the directed force, reaching up to the total force (0.3 N/ms), were achieved by LabVIEW®. Using special force sensors HBM U2B (www.hbm.de); the control system and the produced force are calibrated.

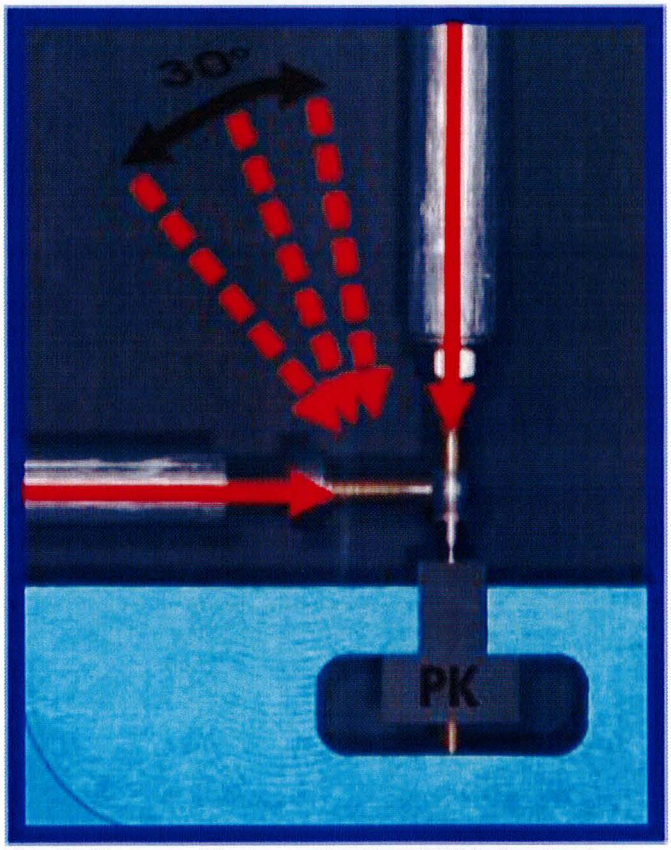

Fig. 19: Close-up of the inspection piece [PK] in the chewing simulator.

2.5 *The radiograph amplifier (RA)*

The radiograph amplifier converts the x-ray projection picture into a picture, of wavelength coverage, of visible light. For the herein described study the image amplifier TH 9438 QX from the company Thales (www.thalesgroup.com) was used. The x-ray meets, after entering the radiograph amplifier, an entrance of a fluorescent screen. Scintillation takes place, when the x-ray is converted into visible light. Directly behind the entrance to the fluorescence screen is a photocathode, which sets electrons free through the arriving visible light. The actual amplification effect arises now. The electrons emitted by the photocathode are carried in an electrical field, starting from 60 keV potential differences, and bundled to a higher energy. Now these electrons, which are withdrawn from the radiograph amplifier, meet an output fluorescent screen, which exhibits a clearly smaller surface than the entrance screen. The electrons are made visible through the passage on the output screen. The amplification factor is indicated for this equipment at 200,000 light quanta per x-ray photon. In illustration 20 the schematic structure of the radiograph amplifier TH 9438 QX is represented.

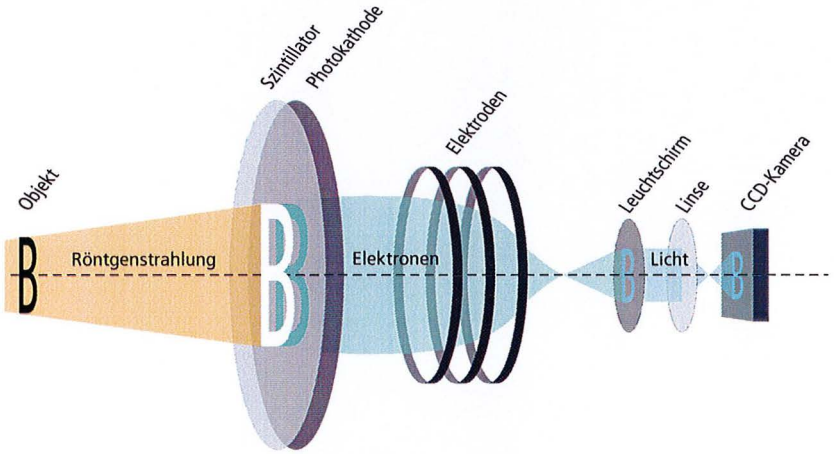

Fig. 20 Schematic structure of the used RA.

2.6 *High speed digital camera*

The radiograph amplifier follows a High-speed digital camera of the type Redlake Motion Pro® HS-3 (www.redlake.de; Fig. 21).

Fig. 21: High speed digital camera Redlake Motion Pro® HS-3.

This type of camera offers an integrated CCD sensor (load Couplet DEVICE sensor). A CCD sensor sends a digital signal proportional to the irradiated quantity of light. The camera is connected by an USB interface to a computer. The digital camera used here can achieve 1000 pictures per second. The arriving signals were "rushed". By averaging each individual pixel, of several one behind the other noted pictures, the signal noise could be reduced. The number of pictures, which are charged with one another, is limited by the arising in-motion unsharpness. The highest image quality was reached with the mean calculation of 11 successive pictures. The calculation of the pictures took place via a developed computer program in LabVIEW® (www.ni.com). Fig. 22 represents an exemplarily calculation of 11 pictures, fig. 23 to a and b in each case a non-calculated and a calculated picture.

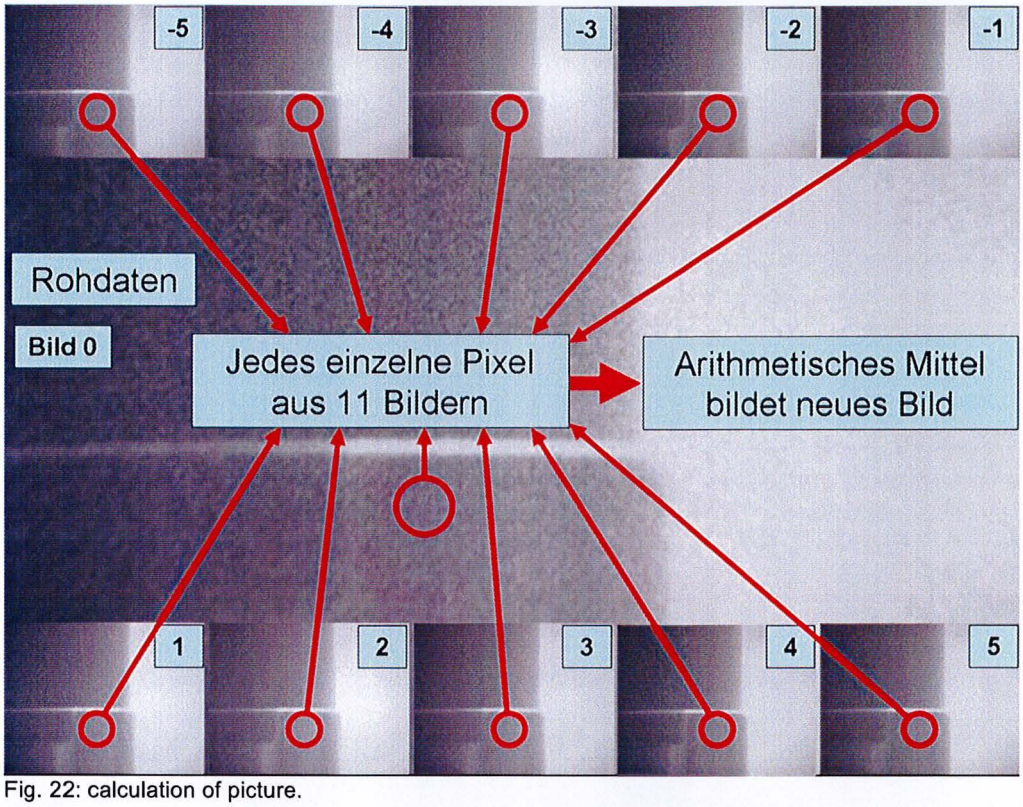

Fig. 22: calculation of picture.

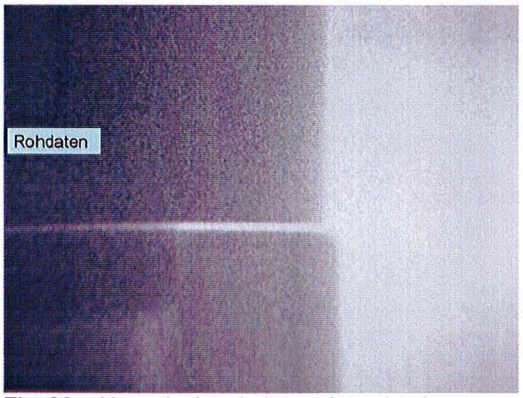

Fig. 23a: Not calculated picture (raw data).

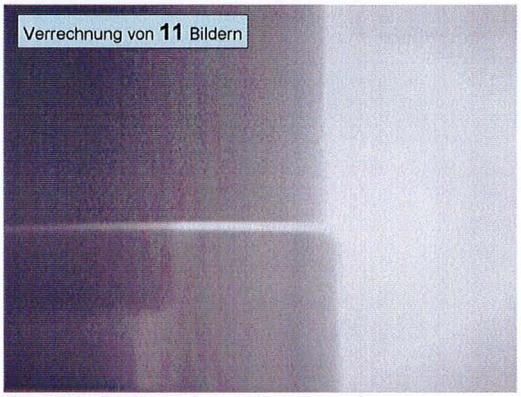

Fig. 23b: Picture after calculation of 11 pictures.

The high image frequency makes for the production of videos, alongside the recording of frames also, possible. The controll of the camera is guaranteed with the help of the graphic programming system LabVIEW® (www.ni.com). The clock frequency, the exposure time and the number of pictures can be adjusted reproducibly. The actuators of the chewing simulator were likewise controlled through and by LabVIEW®, wherein a synchronization of the actuators and the camera took place.

2.7 *Load arrangement*

All inspection pieces were loaded with forces by 25N, 50N, 75N, 100N, 125N, 150N, 175N, 200N. The axial force vector ($\mathbf{F}_{axial}$) was increased up to the, before defined, force. The inclination of the resulting force vector (**F**resultant) from 30° to the implant axis took place via a force application of the horizontal force vector ($\mathbf{F}_{horizontal}$), represented in fig. 24.

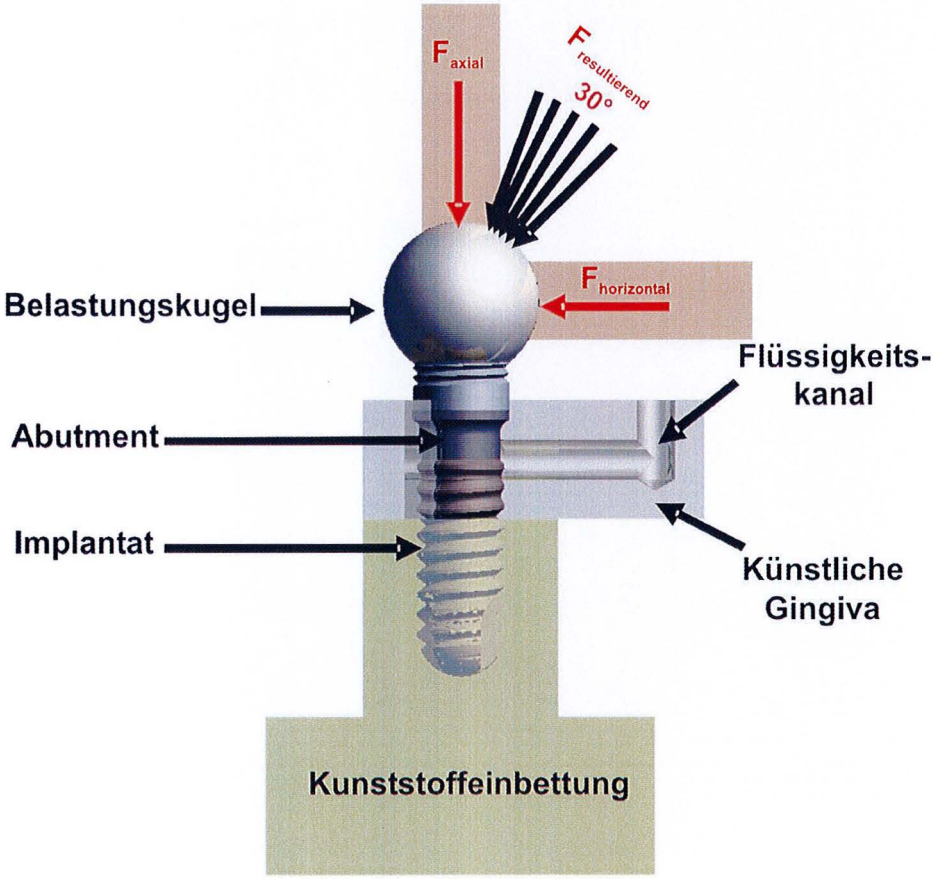

Fig. 24: Schematic representation of the load arrangement.

2.8 Evaluation

The high image frequency makes it possible to provide x-ray videos. For this; every tenth picture was used. The rate of change in the chewing simulator and the produced force, reaching up to the total force amounts of 0.3 N/ms, whereas the rate of change amounts to 0.6 N/ms, to reach the zero point. The period of time that the axial actuator takes to reach the total force amount was equal to the period during the inclination of the force. From this; results the total time of an inspection piece per force cycle. The load cycle determines the recording time of the camera. Synchronization between the actuators and the camera over LabVIEW® under Microsoft Windows XP is not accurate and therefore it was necessary to include an added and an overhanging time for each cycle period. Preliminary tests resulted in an added time of 100 pictures and an overhang time of 1000 pictures. For example a load of 200N results in a load period of 1.66 seconds. The frequency of 1000 pictures, per second, leads to the admission of altogether 2766 pictures. For the production of the x-ray video as "avi.file" with LabVIEW® (www.ni.com) 276 pictures are used after calculations. The x-ray video corresponds to quadruple the slow motion and makes the evaluation of the dynamic processes at the Implant-Abutment-Interface possible. The existence of a possible microgap could be examined by the behaviour of the implant components in the x-ray device. The evaluation of all provided radiographs and x-ray videos were made visually. The visual evaluation of the frames and the provided x-ray videos were evaluated for an existing micro gap between the implant and abutment. Existing cyclic openings and closings of the micro gap could be made visible. In order to measure the developed gap the frame, during and at its' maximum load, was determined. In this frame each pixel inside the gap was counted. According to the resolution of the x-ray video one pixel corresponds to 1,8µm. Therefore the exact size of an existing gap was specified.

3 Results

The results of the here-described study are represented in the following charts. According to the investigational procedure, the occurrence of a micro gap between the implant and the Abutment is shown.

Tab. 3 shows the results of the micro-gap [µm]. For all 5-inspection pieces the starting picture with no load on it and the picture of the 200N load-cycle is shown.

Micro-gap [µm]					
Load	**Inspection piece 1**	**Inspection piece 2**	**Inspection piece 3**	**Inspection piece 4**	**Inspection piece 5**
25N	no space	no space	no space	no space	no space
50N	no space	no space	no space	no space	no space
75N	no space	no space	no space	no space	no space
100N	no space	no space	no space	no space	no space
125N	no space	no space	no space	no space	no space
150N	no space	no space	no space	no space	no space
175N	no space	no space	no space	no space	no space
200N	no space	no space	no space	no space	no space

Tab.3 results of micro gap.

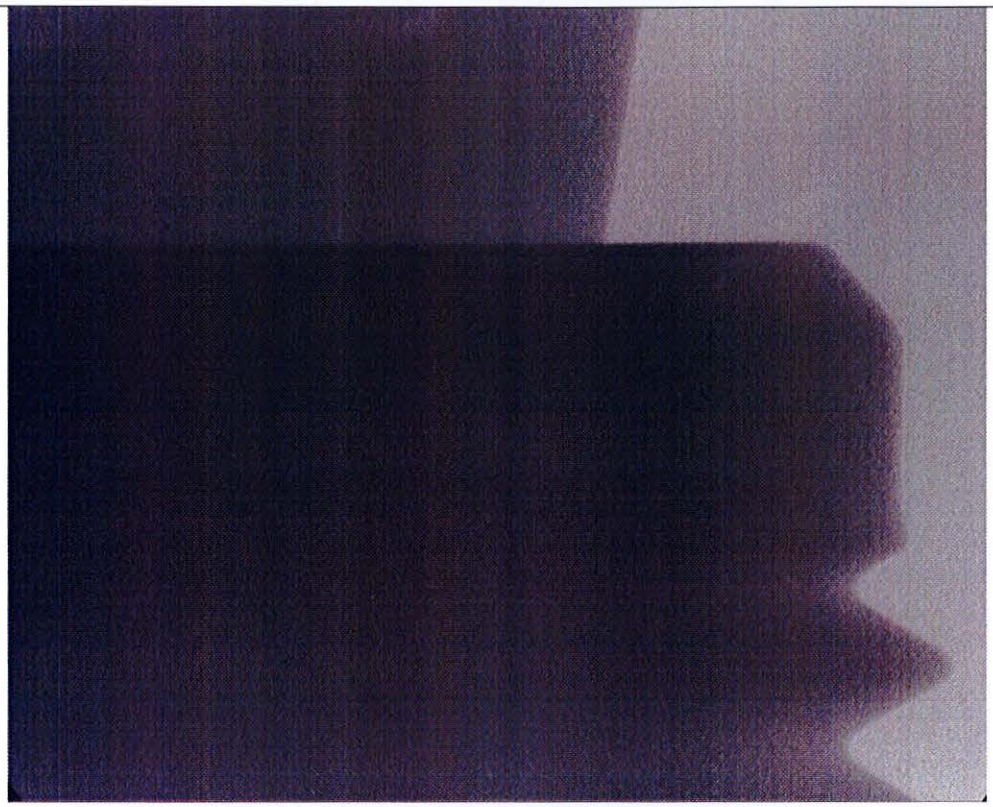

Inspection piece 1 / picture no. 1 / 0N

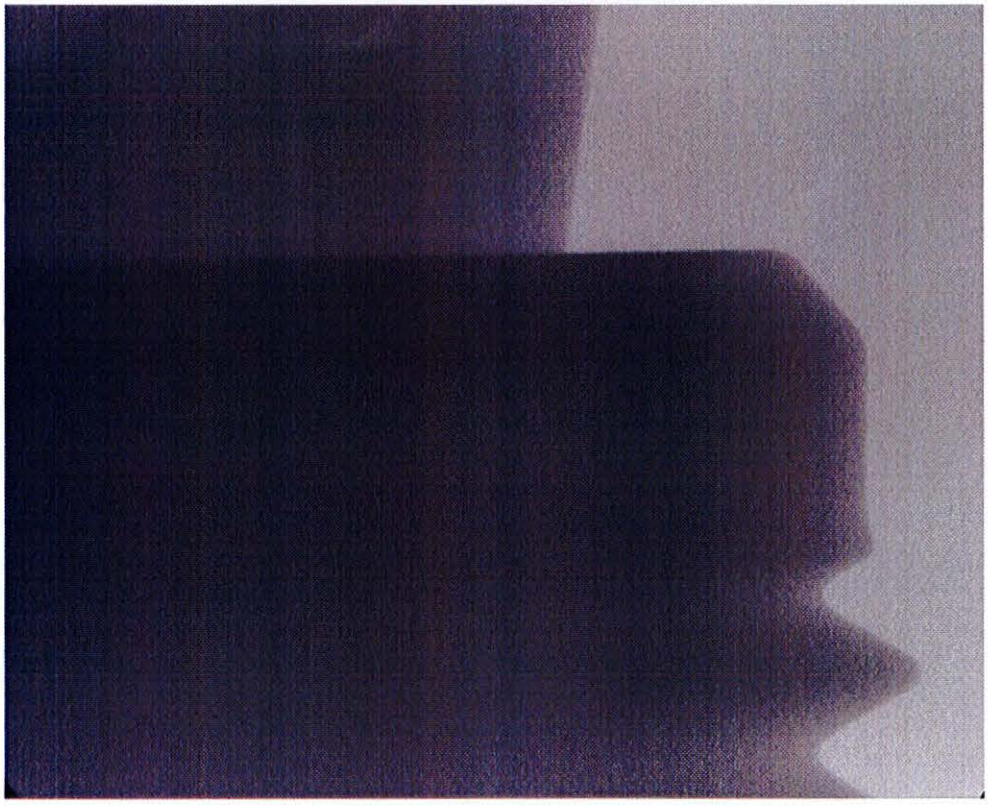

Inspection piece 1 / picture no. 1450 / 200N

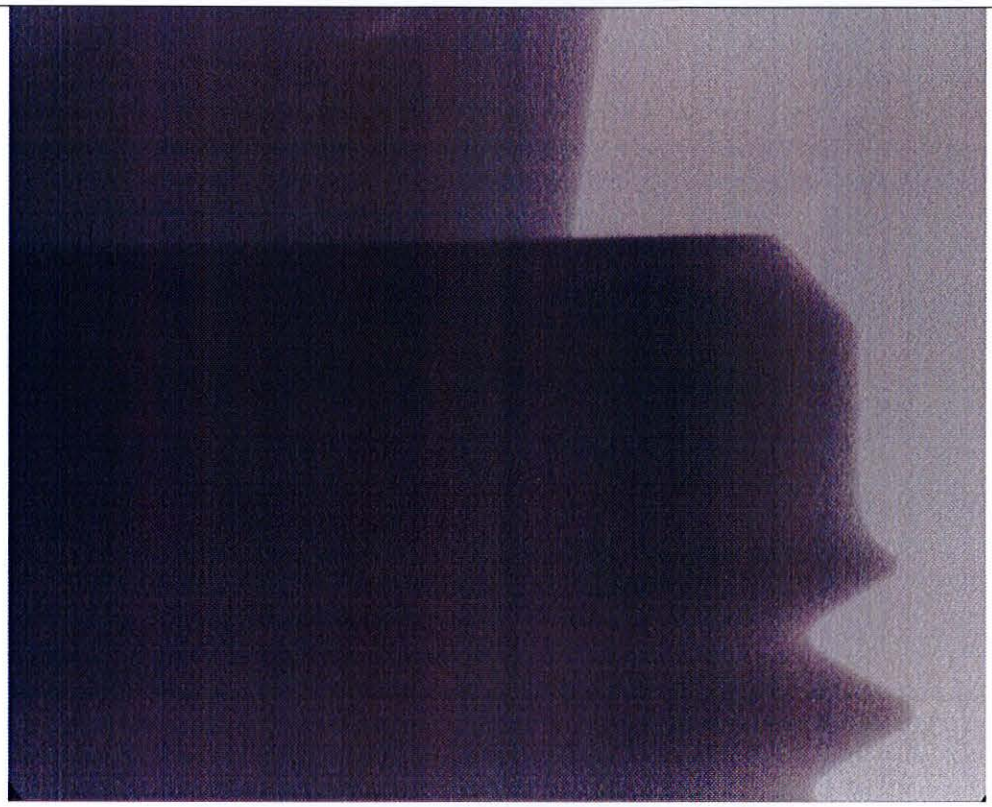

Inspection piece 2 / picture no. 1 / 0N

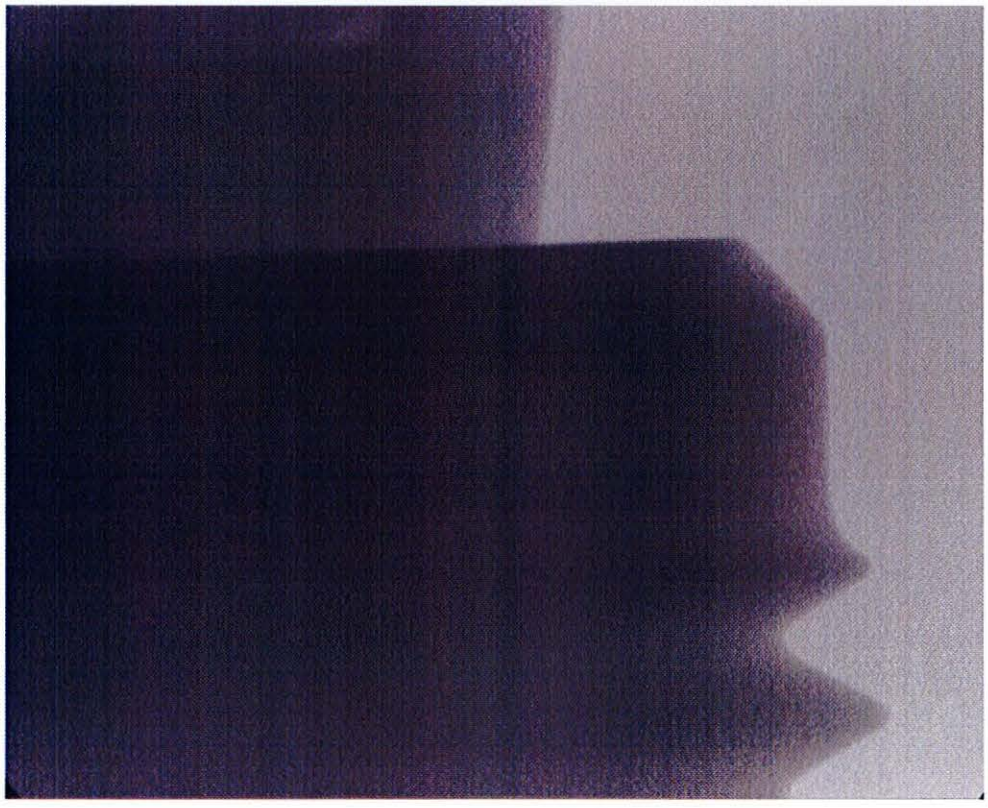

Inspection piece 2 / picture no. 1450 / 200N

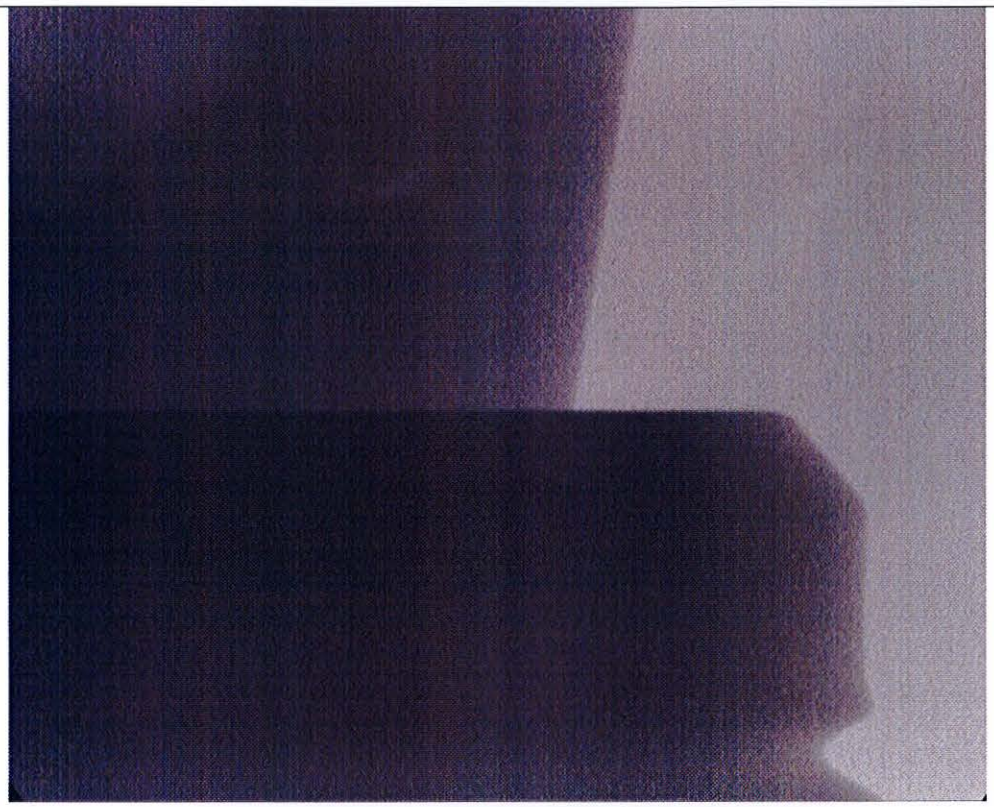

Inspection piece 3 / picture no. 1 / 0N

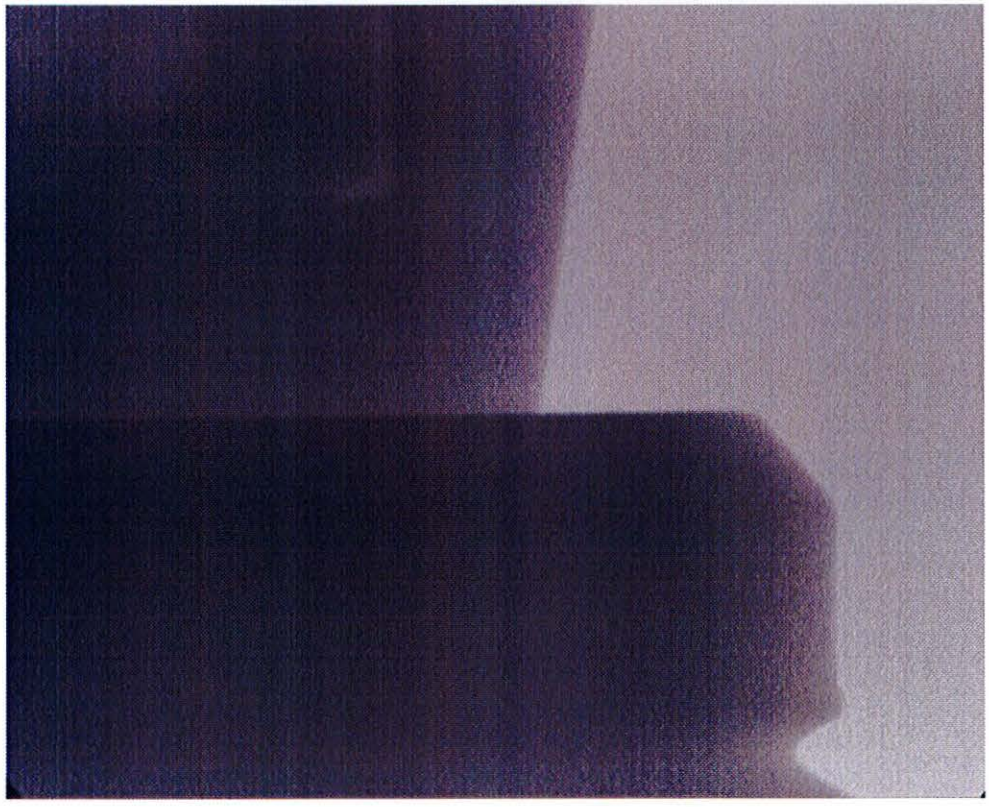

Inspection piece 3 / picture no. 1445 / 200N

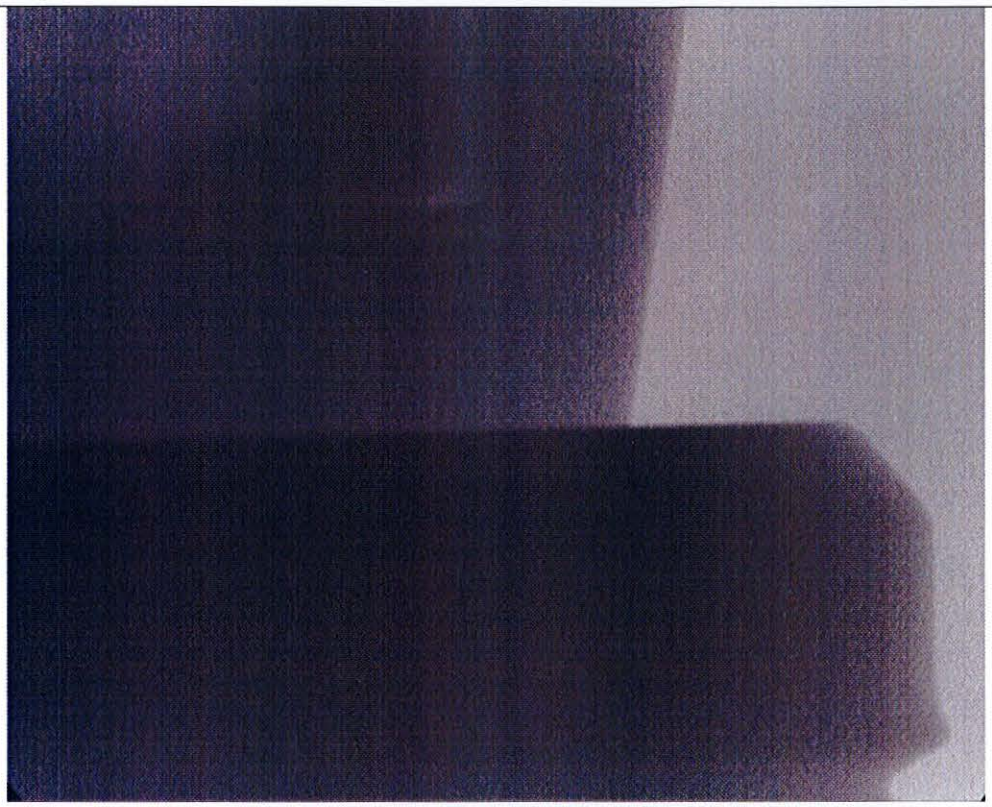

Inspection piece 4 / picture no. 1 / 0N

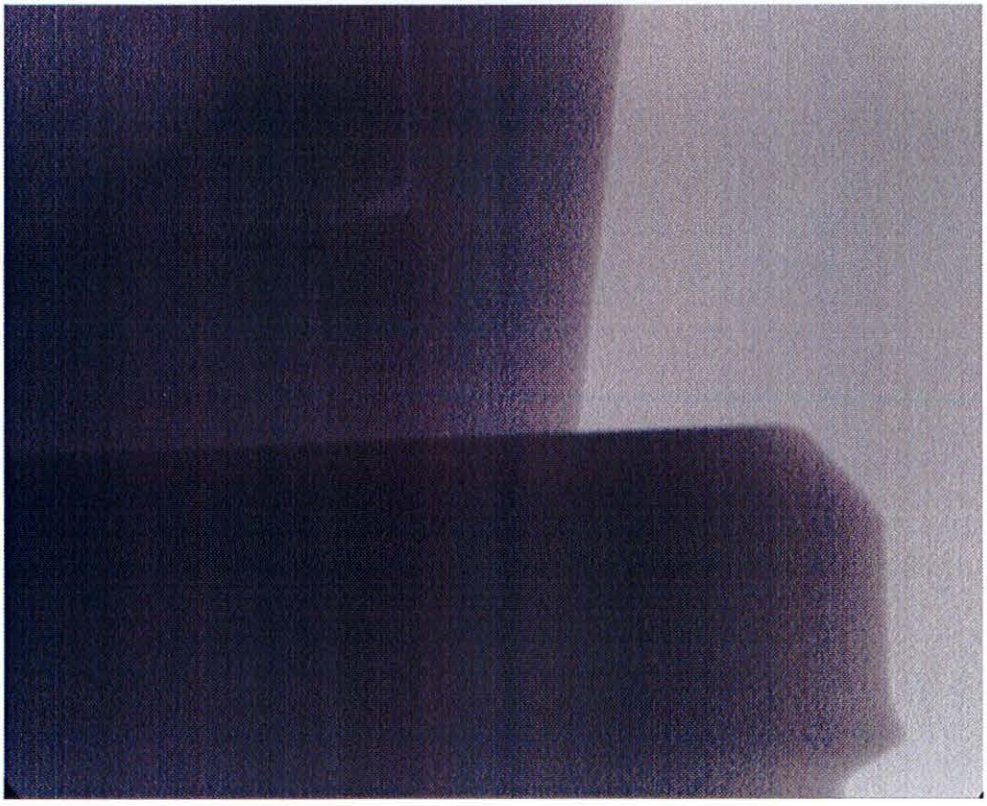

Inspection piece 4 / picture no. 1460 / 200N

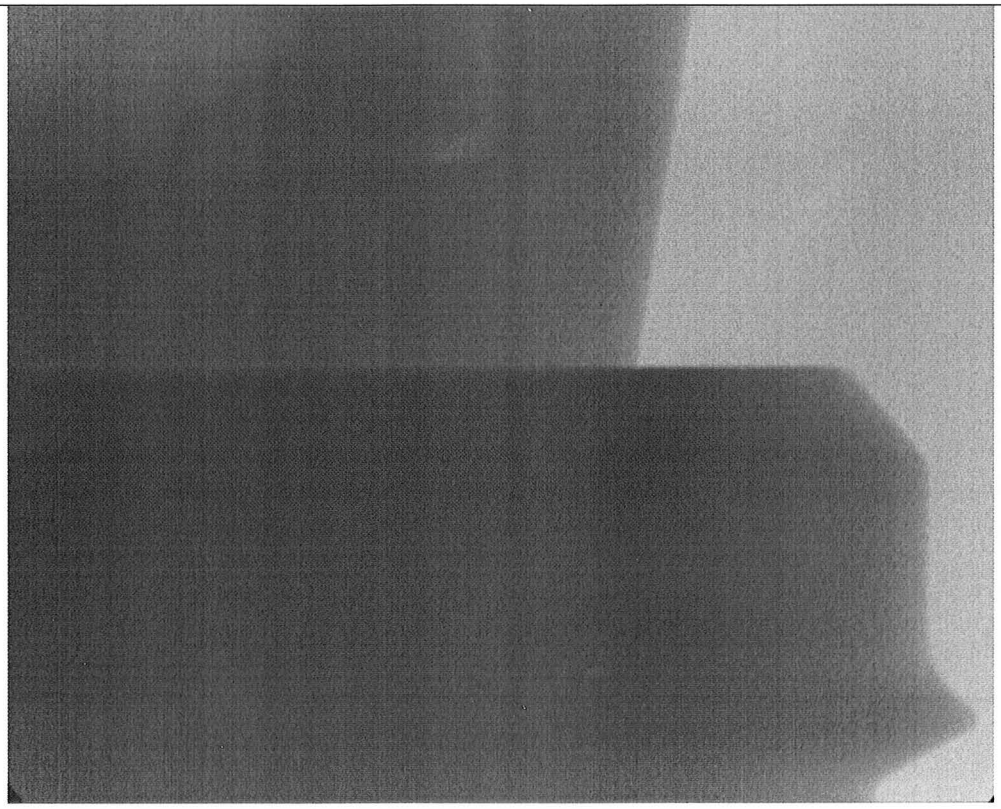

Inspection piece 5 / picture no. 1 / 0N

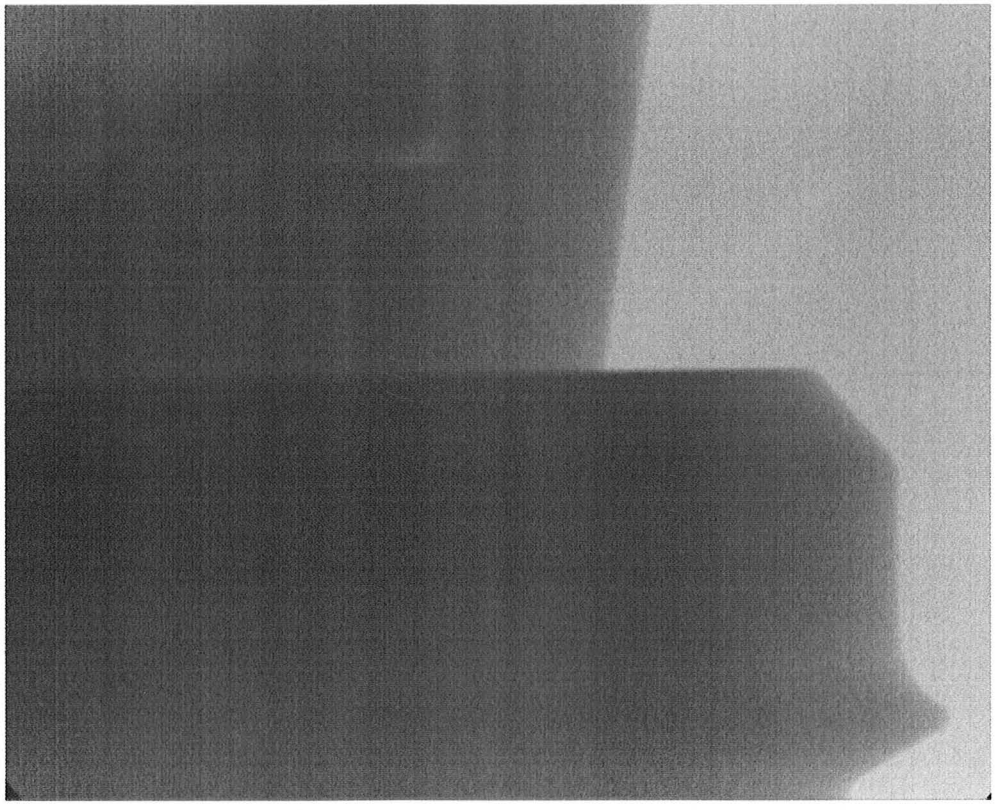

Inspection piece 5 / picture no. 1450 / 200N